Modeling and Simulation of a Surface Micromachined Triaxial Accelerometer

Lijun Jiang, and William N. Carr

New Jersey Institute of Technology, University Heights
Newark, NJ 07102, USA, lj2@njit.edu, carr@adm.njit.edu

ABSTRACT

In this paper, we present the modeling and simulation results of a monolithic triaxial accelerometer. The accelerometer is surface micromachined with fully differential capacitive readout. The mechanical and electrical behaviors of the accelerometer have been simulated and optimized by Finite Element Method (FEM). Static and modal simulations were done to study the static sensitivities and resonant frequencies using ANSYS. The sensing capacitances were analyzed with CoventorWare and compared with a parallel-plate model. The air damping effects are very different for both vertical and lateral moving structures. They were modeled with different analytical models and compared with the simulation results. The effect of the air damping on the dynamic response of the accelerometer is shown.

Keywords: Microaccelerometer, Triaxial Accelerometer, Surface Micromachining, FEM, Capacitive

1 INTRODUCTION

Several monolithic triaxial accelerometers have been fabricated by bulk micromachining [1-4]. In bulk micromachining, a proof mass with height equal to the wafer thickness can be fabricated with relatively high sensitivity. However, portable applications such as medical and biological monitoring require sensors with smaller size and further reduced weight [5]. It has been shown that a triaxial accelerometer can be fabricated with surface micromachining [6]. In standard surface micromachining, several factors set the performance limitations. The proof mass lateral dimensions generally can't exceed several hundred microns. Otherwise it will tend to warp due to the thin film stress. The off-axis rejection is limited by the near unity aspect ratio.

This paper describes the design of a monolithic triaxial accelerometer by surface micromachining. The accelerometer offers smaller size than most previously reported bulk micromachined counterparts [1-4]. It operates in open loop mode, which differs from the triaxial accelerometer in Ref. 6. In this paper, we present modeling and simulation issues in designing the accelerometer. Finite element method simulations have been used in both mechanical and electrical designs. Different air damping for vertical and lateral moving mass were modeled and compared with simulations.

2 SENSOR STRUCTURE

The triaxial accelerometer consists of three independent mass-spring structures. Fig.1 shows the schematic view of the z-axial and lateral structure. The lateral structure for both x-axis and y-axis are identical but aligned at 90 degree to each other. Each proof mass is 200um×200um, suspended with folded beam springs. The gap between the proof mass and the substrate is about 1.2um.

The sensing of the accelerometer is capacitive. In our accelerometer, we implemented fully differential readout for both the z- and lateral structures. As shown in Fig.2(a), two parallel-plate capacitors were used for z-axial accelerometer. When the proof mass is deflected from its neutral position, both capacitors will increase or decrease depends on the acceleration direction. Two separate reference capacitors are used to implement fully differential readout. The sensing capacitors for x- and y-axes are formed with two series of interdigital electrodes (Fig.2(b)). They can be modeled with two lumped variable area parallel plate capacitors. When the accelerometer senses the acceleration in lateral axes, the two capacitors, C_{x1} and C_{x2}, will vary oppositely in magnitude. The equivalent electrical models for the fully differential readouts are illustrated in Fig.3. The reference capacitors C_r are fabricated on the same substrate but with fixed suspension and will not vary with accelerations.

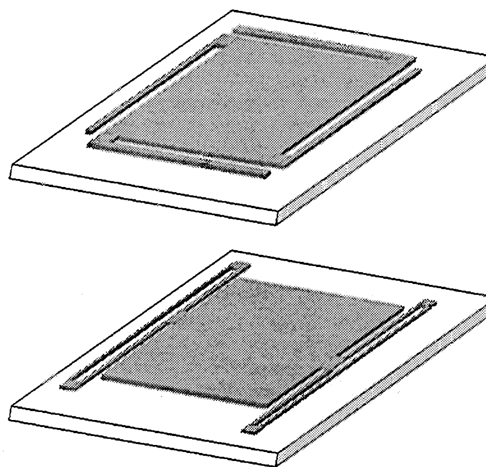

Fig.1: Schematic view of the triaxial accelerometer: (top) z-axial structure, (bottom)x,y-axial

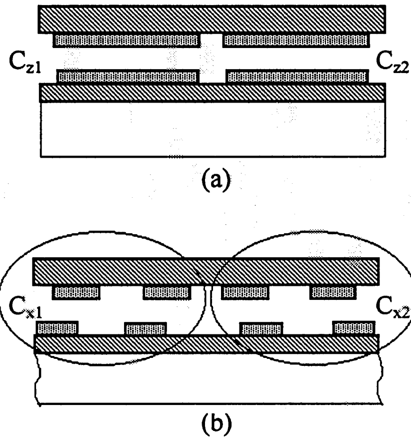

Fig.2: A cross section view of the sensing capacitors arrangement of the triaxial accelerometer (a) z-axial device (b) x,y-axial devices

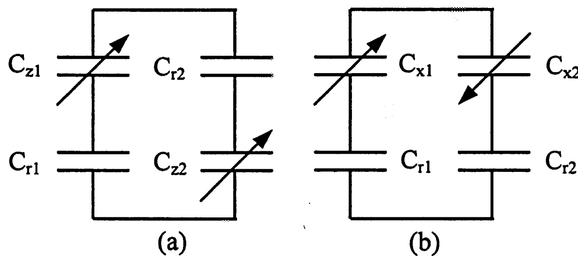

Fig.3: Equivalent electrical model of the fully differential readout of the triaxial accelerometer (a) z-axial (b) x,y-axial

3 DESIGN AND SIMULATION

Comparable parameters should be designed for three separate mass-spring structures. There is tradeoff between the sensitivity and the bandwidth of the accelerometer. For a quasi-static accelerometer, the sensitivity is given by

$$S = \frac{x}{a} = \frac{m}{k} = \frac{1}{\omega_0^2} \quad (1)$$

where the m is the proof mass, k is the spring constant of the suspension beam, ω_0 is the resonant frequency. The resonant frequency defines the maximum bandwidth of the accelerometer including readout circuitry. To increase the sensitivity, a more compliant spring should be used. But it can't be too compliant otherwise the bandwidth and the shock resistance will not meet the useful system specs.

3.1 Spring Design and Static Simulations

Folded beam springs are used for both z- and lateral structures. The folded beam design can save the space and release the residual stress. The analytical formula for the spring constants of various forms of folded beam structures were given in [7]. With the dimensions derived from the analytical formula, a finite element model is created for each axial sensor in ANSYS 5.7. To evaluate the static sensitivity, an acceleration is applied in its main sensitive axis. Fig.4 shows the deflections of the accelerometer under 1G ($9.8 m/s^2$) acceleration for both z- and x,y-axes. The cross-axial sensitivity is studied by comparing the deflection of the proof mass under acceleration in two other axes than the sensing axis. It was shown that the beams in the z-axial accelerometer make it sensitive only to the vertical signal. However, the limited aspect ratio makes the x- and y- structures also sensitive to accelerations in z direction. It can be shown that the off-axial acceleration can be rejected to first order by the fully differential readout arrangement (section 3.3). The air damping effect will also improve the off-axial rejection.

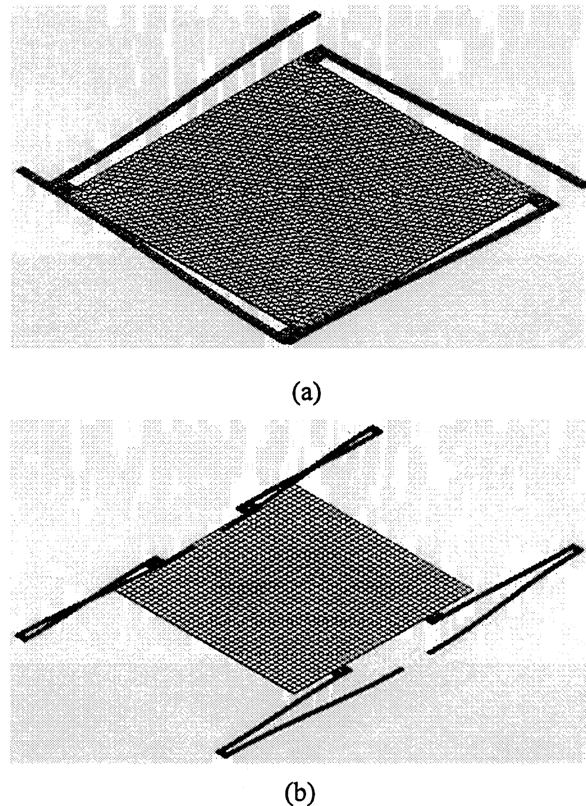

Fig.4: FEM simulated response of the triaxial accelerometer under 1G acceleration along the sensing axis (a) z-axial (b) x,y-axial

3.2 FEM Modal Simulations

The modal simulations give the resonant frequencies of the accelerometer. The undamped modal simulation with ANSYS was carried out on the same solid model as that used in static analysis. The simulation results were listed in Table1. It was seen that the 1st resonant mode for the z-axis is larger than the x,y-axes due to the stiffer spring.

Table1: Resonant frequencies of the accelerometer from ANSYS modal simulations

	z-axis	x, y-axes
1st mode	13.73 kHz	4.86 kHz
2nd mode	24.93 kHz	9.55 kHz
3rd mode	24.97 kHz	9.98 kHz
4th mode	262.8 kHz	15.24 kHz

3.3 FEM Electrostatic Simulations

The capacitors oriented for z-axis sensitivity can be modeled with parallel-plate capacitors. The capacitance variation of a parallel-plate capacitor is given by:

$$\Delta C = \frac{\varepsilon A}{d^2} \cdot \Delta d \tag{2}$$

where the A is the electrode area, d is the gap between the upper and lower electrodes. However, for the x,y-axial capacitors, the fringe field effect must be considered. Electrostatic simulation is needed to give more accurate results. This simulation was done with CoventorWare 2001. It reveals that the z-axial capacitors can be well modeled by parallel-plate model. Fig.5 shows the change of the capacitance with the deflection of the electrode from its rest position including fringe field effects.

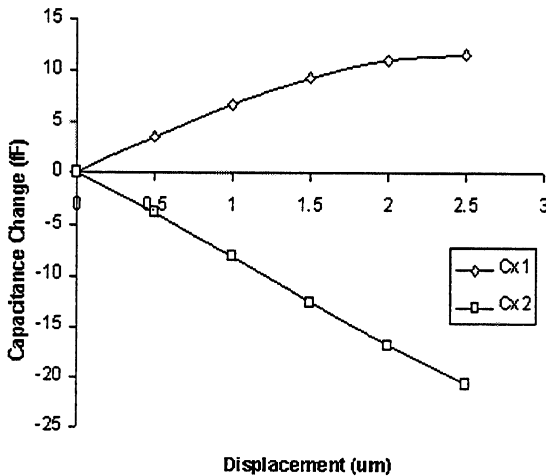

Fig.5: Total capacitance change of the x,y-axial devices with the displacement of the proof mass from its resting position

4 ACCELEROMETER DYNAMICS

The study of the dynamic of the accelerometer was concentrated on the air damping effect. Due to the micro-sizing in MEMS devices, the fluid dynamics differ from the macroscopic world. Sometimes, effects such as slip flow, rarefaction, intermolecular forces and other effects may have to be considered. The gas damping in MEMS can be modeled by either continuum models or molecular models. In this section, the analytical models based on simplified Navier-Stokes equation are presented first. The MemDamping program is then used to simulate the damping effects.

4.1 Squeeze-Film Damping

For vertical movement of the proof mass in the z-axial device, the squeeze-film damping provides the main damping mechanism [8]. The damping comes from the pressure built-up inside the gap when the proof mass moves vertically. The Navier-Stokes equation can be simplified into Reynold's equation under several assumptions. Firstly, we assume incompressible flow of the gas and ignore the inertial effects. Secondly, we assume that the gas velocity in the z-axis is a linear function of z only. With no-slip boundary conditions, we get the reduced Reynold's equation:

$$\frac{\partial^2 P}{\partial x^2} + \frac{\partial^2 P}{\partial y^2} = \frac{12\mu}{h_0^3} \cdot \frac{\partial h}{\partial t} \tag{3}$$

where the P is the gas film pressure, u is the gas viscosity, h_0 is the gap when the proof mass is at its rest position.

The above equation can be solved for simple geometries. For rectangular plate with length 2L and width 2W, the damping force derived from Eq.3 is [8]:

$$F_d = \frac{16 f\left(\frac{W}{L}\right) \cdot W^3 L}{h_0^3} \cdot \frac{\partial h}{\partial t} \tag{4}$$

where $f(W/L)$ is a function of W/L ratio and equals 0.427 for W=L. Finally, the damping coefficient b is derived from the damping force over the moving velocity of the proof mass:

$$b = 0.427 \mu \frac{L^4}{h_0^3} \tag{5}$$

4.2 Slide-Film Damping

For the laterally moving plate structures like the x,y-accelerometers in this paper, the air damping results from viscous dragging of the ambient gas, termed as slide-film damping. Previous studies have been based on Couette flow

and Stokes flow model [9,10]. Quality factors have been derived analytically with some assumptions [10]:

$$\frac{1}{Q} = \frac{1}{Q_{cd}} + \frac{1}{Q_{sd}} \tag{6}$$

where the Q_{cd} and Q_{sd} are due to the Couette-flow on the top surface of the proof mass and Stokes-flow under the plate respectively:

$$\begin{aligned} Q_{cd} &= \frac{kh_0}{2\pi\omega_0 \mu A_{eff}} = \frac{h_0}{\mu A_{eff}}\sqrt{km} \\ Q_{sd} &= \frac{k\delta}{2\pi\omega_0 \mu A_{eff}} = \frac{\delta}{\mu A_{eff}}\sqrt{km} \end{aligned} \tag{7}$$

where A_{eff} is the effective area, δ is the penetration depth.

4.3 Simulation of the Air Dampings

MemDamping [11] program was used to simulate the air damping. It's a hybrid Navier-Stokes-Reynold's solver, taking into consideration of the effects of spring and edge and vent holes. Fig.6 shows the simulation results under 1 atm air pressure. At low frequency, the z-structure is over-damped by the squeeze-film damping. With increasing frequency, the spring effect dominates. We found that at the same pressure, the damping in z-axis is almost four orders higher than that of the x,y-axes. Different dynamics are expected due to the different dampings.

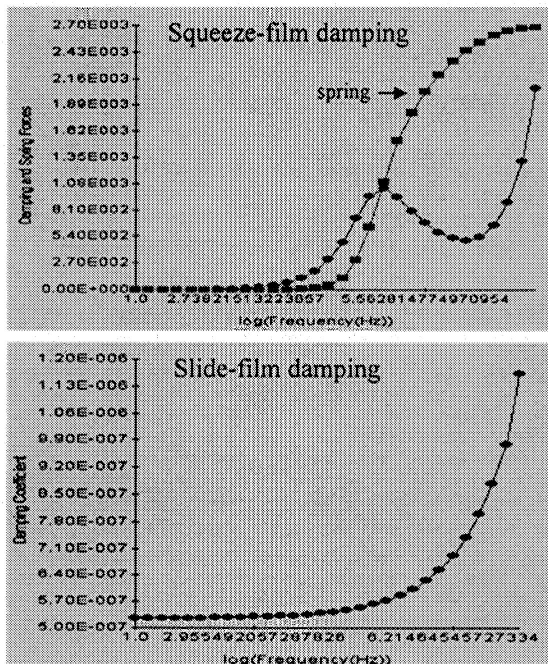

Fig.6: The simulated damping coefficients and spring constant due to the air (top) z-axis (bottom) x,y-axes

5 CONCLUSION

A monolithic capacitive triaxial accelerometer has been designed. The mechanical and electrical behaviors of the accelerometer were simulated with finite element methods using ANSYS 5.7 and CoventorWare 2001. We confirm the feasibility for a triaxial accelerometer by surface micromachining and reasonable off-axial rejection. The accelerometer has been fabricated and is currently under test.

REFERENCES

[1] R. Puers, and S. Reyntjens, "Design and processing experiments of a new miniaturized capacitive triaxial accelerometer," Sensors and Actuators A, 68, 324-328, 1998

[2] K. Kwon, and S. Park, "A bulk-micromachined three-axis accelerometer using silicon direct bonding technology and polysilicon layer," Sensors and Actuators A, 66, 250-255, 1998

[3] S. Butefisch, A. Schoft, and A. Buttgenbach, "Three-axes monolithic silicon low-g accelerometer," J. MEMS, 9 (4), 551-556, 2000

[4] G. Li, Z. Li, C. Wang, Y. Hao, T. Li, D. Zhang, and G. Wu, "Design and fabrication of a highly symmetrical capacitive triaxial accelerometer," J. Micromech. Microeng., 11, 48-54, 2001

[5] C. V. C. Bouten, K. T. M. Koekkoek, M. Verduin, R. Kodde, and J. D. Janssen, "A triaxial accelerometer and portable data processing unit for the assessment of daily physical activity," IEEE Tran. Biomed. Eng., 44 (3), 136-147, 1997

[6] M. Lemkin, and B. E. Boser, "A three-axis micromachined accelerometer with a CMOS position-sense interface and digital offset-trim electronics," IEEE JSSC, 34 (4), 456-468, 1999

[7] G. Fedder, "Simulation of microelectromechanical systems," doctoral dissertation, Univ. of California at Berkeley, 1994

[8] J. B. Starr, "Squeeze-film damping in solid-state accelerometers," Tech. Digest, IEEE Solid State Sensors and Actuators Workshop, Hilton Head Island, SC, 44-47, June 1990

[9] Y. H. Cho, B. M. Kwak, A. P. Pisano, and R. T. Howe, "Viscous energy dissipation inn laterally oscillating planar microstructures: a theoretical and experimental study," Proc. IEEE Workshop on MEMS, 93-98, 1993

[10] X. Zhang, and W. C. Tang, "Viscous air damping inn laterally driven microstructures," Proc. IEEE Workshop on MEMS, 199-204, 1994

[11] Analyzer supplemental tutorials and reference guide, CoventorWare 2001, Coventor Inc., 4001 Weston Parkway, Cary, NC